Published in final edited form as:
Bioconjug Chem. 2010 October 20; 21(10): 1794–1803. doi:10.1021/bc100091q.

Annexin A5-Functionalized Bimodal Nanoparticles for MRI and Fluorescence Imaging of Atherosclerotic Plaques

Geralda A. F. van Tilborg[*,†,‡], **Esad Vucic**[§], **Gustav J. Strijkers**[†], **David P. Cormode**[§], **Venkatesh Mani**[§], **Torjus Skajaa**[§], **Chris P. M. Reutelingsperger**[‖], **Zahi A. Fayad**[§], **Willem J. M. Mulder**[§], and **Klaas Nicolay**[†]

[†]Biomedical NMR, Department of Biomedical Engineering, Eindhoven University of Technology, Eindhoven, The Netherlands [‡]Image Sciences Institute, University Medical Center Utrecht, Utrecht, The Netherlands [§]Translational and Molecular Imaging Institute, Mount Sinai School of Medicine, New York, New York [‖]Cardiovascular Research Institute Maastricht, Maastricht University, Maastricht, The Netherlands

Abstract

Apoptosis and macrophage burden are believed to correlate with atherosclerotic plaque vulnerability and are therefore considered important diagnostic and therapeutic targets for atherosclerosis. These cell types are characterized by the exposure of phosphatidylserine (PS) at their surface. In the present study, we developed and applied a small micellar fluorescent annexin A5-functionalized nanoparticle for noninvasive magnetic resonance imaging (MRI) of PS exposing cells in atherosclerotic lesions. Annexin A5-mediated target-specificity was confirmed with ellipsometry and in vitro binding to apoptotic Jurkat cells. In vivo T_1-weighted MRI of the abdominal aorta in atherosclerotic ApoE$^{-/-}$ mice revealed enhanced uptake of the annexin A5-micelles as compared to control-micelles, which was corroborated with ex vivo near-infrared fluorescence images of excised whole aortas. Confocal laser scanning microscopy (CLSM) demonstrated that the targeted agent was associated with macrophages and apoptotic cells, whereas the nonspecific control agent showed no clear uptake by such cells. In conclusion, the annexin A5-conjugated bimodal micelles displayed potential for noninvasive assessment of cell types that are considered to significantly contribute to plaque instability and therefore may be of great value in the assessment of atherosclerotic lesion phenotype.

INTRODUCTION

Annexin A5, a 36 kDa protein belonging to the annexin family, is known to bind to the negatively charged phospholipid phosphatidylserine (PS) in the presence of Ca^{2+} (1, 2). In almost all homeostatic cells, this phospholipid is restricted to the cytoplasmic leaflet of the plasma membrane and therefore inaccessible from the extracellular compartment (3). However, dying and activated cells, such as apoptotic cells, activated platelets (4, 5), and activated macrophages (6), are known to expose PS also in the exoplasmic layer of the cell membrane. Furthermore, membrane integrity is lost during the process of necrosis, thereby allowing extracellular proteins to enter the cell (7). Therefore, annexin A5 has been proposed and exploited to function as a ligand to target apoptotic, necrotic, and other PS

[*]Corresponding author. Geralda A. F. van Tilborg, Image Sciences Institute, University Medical Center Utrecht, Yalelaan 2, 3584 CM Utrecht, The Netherlands. Phone: +31 30 2535515. gtilborg@gmail.com.

exposing cells for a variety of applications, including cell sorting, imaging, and drug targeting (8–11).

In atherosclerosis, a high occurrence of apoptosis and necrosis, as well as high macrophage burden, is believed to contribute significantly to plaque vulnerability and rupture (12–15). Consequently, identification of these markers using annexin A5-targeted noninvasive diagnostic imaging may contribute to discrimination between atherosclerotic lesions with a stable and unstable phenotype, which would be of great clinical value. To this aim, there have been a number of studies where technetium (^{99}Tc) or indium (^{111}In) -labeled annexin A5 has been used for imaging of vulnerable plaque or the effect of therapy with nuclear techniques in both experimental (16–20) and human atherosclerosis (21). Importantly, these studies demonstrated significant correlations between the extent of annexin A5 uptake, macrophage content, and the amount of apoptosis. Furthermore, all of these values were shown to increase with more advanced lesions, as classified according to the American Heart Association.

Although nuclear imaging is a very sensitive technique, it suffers from poor spatial resolution and the images lack detailed anatomical information. MRI is an imaging modality with a high spatial resolution and can discriminate among different plaque components (22). Nevertheless, MRI suffers from relatively low sensitivity (23). In targeted molecular MRI, the latter drawback is frequently compensated for by using high relaxivity (super)-paramagnetic imaging probes (24). These probes, usually nanoparticulate in nature, contain either (multiple) iron oxide crystals or a high payload of gadolinium. We and others previously reported on a number of such nanoparticles that have been successfully applied for MRI-based molecular imaging of atherosclerosis. These include target-specific lipid-based nanoparticles within the size range of 10–300 nm, such as micelles (25, 26), high-density lipoproteins (HDL) (27), liposomes (28), and microemulsions (29), in which large numbers of Gd-DTPA moieties were incorporated in the lipid (bi)layer. Alternatively, iron oxide-based nanoparticles have been developed to enable molecular MRI of lipoproteins (30) or adhesion molecule expression in atherosclerotic plaques (31). For validation and co-localization purposes, the aforementioned nanoparticles can include additional fluorescent dyes, such as fluorescent lipids or quantum dots (32).

In the present study, we developed and characterized a small annexin A5-conjugated micellar nanoparticle, carrying multiple Gd-labeled lipids for MRI and fluorescent lipids for fluorescence microscopy or imaging. Target-specificity of this nanoparticle for PS was examined with ellipsometry of PS-containing membranes, as well as CLSM of apoptotic Jurkat cells in vitro. Furthermore, in a pilot study, the nanoparticles were applied for in vivo MR imaging of phosphatidylserine exposing cells in atherosclerotic lesions of ApoE knockout (ApoE$^{-/-}$) mice. Ex vivo near-infrared fluorescence imaging of intact aortas was used to validate and quantify nanoparticle uptake in the lesions, while CLSM was employed to investigate which specific cell types bound the contrast agent.

EXPERIMENTAL PROCEDURES

Materials

1,2-distearoyl-*sn*-glycero-3-phosphoethanolamine-*N*-[methoxy(poly(ethylene glycol))-2000] (PEG2000-DSPE), 1,2-distearoyl-*sn*-glycero-3-phosphoethanolamine-*N*-[maleimide-(poly(ethylene glycol))2000] (Mal-PEG2000-DSPE), 1,2-distearoyl-*sn*-glycero-3-phosphoethanolamine-*N*-[amino(poly(ethylene glycol))2000] (Amine-PEG2000-DSPE), and 1,2-dioleoyl-*sn*-glycero-3-phosphoethanolamine-*N*-(lissamine rhodamine B sulfonyl) (Rhodamine-PE) were obtained from Avanti Polar Lipids (Albaster, AL). Cy5.5 monoreactive NHS ester was obtained from GE Healthcare Europe GmbH (Amersham

CyDye value packs, Diegem, Belgium). Gd-DTPA-di(stearylamide) (Gd-DTPA-DSA) was purchased from Gateway Chemical Technology (St. Louis, MO). HEPES was purchased from Merck (Darmstadt, Germany). All other chemicals were of analytic grade or of the best grade available. A Bradford protein assay kit was purchased from Bio-Rad laboratories (Veenendaal, The Netherlands).

Cy5.5-PEG2000-DSPE

Cy5.5-PEG2000-DSPE lipid was prepared by covalent conjugation of Cy5.5 monoreactive NHS ester to micellar Amine-PEG2000-DSPE. First, Amine-PEG2000-DSPE micelles were prepared by lipid film hydration. In short, 10 μmol Amine-PEG2000-DSPE was dissolved in 0.5 mL chloroform. Subsequently, a lipid film was obtained by rotary evaporation of the solvent, followed by additional drying under nitrogen flow. Next, the film was gently hydrated in 5 mL sodium bicarbonate solution (0.1 M $NaHCO_3$, pH 8.0) at 65 °C, until a clear solution was obtained. Once micelles were formed, 5 mg Cy5.5 monoreactive NHS ester was dissolved in 100 μL dimethyl sulfoxide (DMSO) and immediately added to the micelle-containing suspension. Coupling was performed via overnight incubation at 4 °C on a moving table. The resulting micelles were sequentially concentrated and resuspended in ultrapure water, using 20 mL vivaspin concentrators (Vivascience, Sartorius Stedim Biotech, 10 000 MWCO) at 3000 × *g* and 4 °C. At least five wash cycles were required to remove nonbound Cy5.5. Following the washing procedure, the Cy5.5-PEG2000-DSPE-micelle suspension was dried with a FreeZone 4.5 L benchtop freeze–dry system for three days (Labconco). The obtained lipid powder was dissolved in a 2:1 (v/v) mixture of chloroform and methanol, to a final Cy5.5-PEG-DSPE concentration of 1 μmol/mL.

Micellar Contrast Agent

Bimodal micelles were obtained by lipid film hydration of a lipid mixture, typically containing a total amount of 50 μmol lipids. Gd-DTPA-DSA, PEG2000-DSPE, and Mal-PEG2000-DSPE were added at a molar ratio of 0.5/0.4/0.1 and dissolved in chloroform/methanol 2:1 (v/v). Next, 1 mol % Cy5.5-PEG-DSPE or Rhodamine-PE was added to the lipid mixture for near-infrared fluorescence imaging or confocal microscopy, respectively. The solvent was removed by rotary evaporation, and additional drying of the lipid film was performed under nitrogen flow. Next, the lipid film was gently dissolved in 4 mL of warm HEPES buffered saline (20 mM HEPES and 135 mM NaCl, pH 6.7, 65 °C) during continuous heating at 65 °C until a clear solution was obtained.

Annexin A5 Coupling

The micellar contrast agent was functionalized with a variant of annexin A5 that has a single cysteine residue in the N-terminal tail (annexin A5-cys). The PS and apoptotic cell binding properties of annexin A5-cys are identical to those of recombinant human annexin A5 as previously shown by ellipsometry (1) and flow cytometry (33), respectively. Annexin A5-cys (~36 kDa) was covalently conjugated to the Mal-PEG2000-DSPE-containing micelles by sulfhydryl–maleimide coupling, as previously described for other lipid-based agents (34). In short, annexin A5-cys was reactivated with 10 mM DTT for 1.5 h at 37 °C. Next, 10 mM EDTA was added and DTT and EDTA were removed by extensive dialysis using a 12–14 kDa membrane (Pierce). Activated annexin A5-cys was added to the micelle suspension at a final concentration of 750 μg/μmol total lipid, and coupling was performed overnight at 4 °C. Subsequently, the annexin A5-micelles (AnxA5-micelles) were concentrated and resuspended at least 5 times in HEPES buffered saline (20 mM HEPES and 135 mM NaCl, pH 6.7) to remove nonconjugated annexin A5-cys, using 20 mL vivaspin concentrators (Vivascience, Sartorius Stedim Biotech, MWCO 100 000) at 3000 × *g* and 4 °C. Untargeted micelles were concentrated using the same protocol. A schematic of the preparation procedure of the annexin A5-micelles is shown in Figure 1.

Contrast Agent Characterization

Dynamic light scattering was performed on a Malvern instrument (Zetasizer, Nano-S) to determine the hydrodynamic diameter of control and anxA5-micelles in HEPES buffered saline (20 mM HEPES and 135 mM NaCl, pH 7.4), as deduced from the intensity-weighted particle size distribution. Final micelle concentration was determined by a phosphate analysis according to Rouser (35) after complete destruction with perchloric acid. Protein content of the AnxA5-micelles was measured according to a modified Bradford method (36), which corrects for lipid-associated background absorption at 750 nm by adding equivalent concentrations of control-micelles to calibration samples containing a known amount of annexin A5-cys. Relaxivity measurements were performed on a 60 MHz table top NMR spectrometer (Bruker, Minispec), at 25 and 37 °C. Relaxivities were obtained by measuring T_1 and T_2 values for serial dilutions of the Cy5.5-labeled micelles in the range 0.4–3.4 mM total lipid. T_1 relaxation times were obtained with an inversion recovery sequence, whereas T_2 values were measured using a CPMG sequence.

In Vitro Targeting

Ellipsometry—The interaction of the Cy5.5-labeled annexin A5-micelles with phosphatidylserine (PS) was monitored with ellipsometry as described in detail elsewhere (34). Untargeted micelles and unconjugated annexin A5-cys served as a control. In short, a silica plate was coated with a lipid bilayer of PS and phosphatidylcholine (PC) at a molar ratio of 20:80. The lipid-coated silica plate was placed in a sample container, filled with 5 mL of Ca^{2+}-containing binding buffer (10 mM HEPES, 150 mM NaCl, 5 mM KCl, 1 mM $MgCl_2$, 2.5 mM $CaCl_2$, pH 7.4). Micelles were added at a final concentration of 280 μM total lipid, while the final concentration of free annexin A5-cys protein was 56 nM. Binding of the particles was assessed by continuously measuring the polarization angle of the reflected elliptically polarized light. Once the polarization angle reached a steady-state value, 5 mM EDTA was added to investigate Ca^{2+}-dependent membrane association.

Apoptotic Cells—Target specificity for apoptotic cells was examined in the T-lymphoma cell line Jurkat (ATCC). Cells were grown in RPMI1640 medium (Gibco) at 37 °C in a humidified atmosphere and 5% CO_2. Medium was supplemented with 10% fetal calf serum and a mixture of antibiotics (100 units/mL penicillin and 0.1 mg/mL streptomycin; Biochrom AG). In order to induce a high level of apoptosis, Jurkat cells were resuspended to 1×10^6 cells/mL medium and treated with 200 ng/mL anti-Fas (CD95 human monoclonal antibody, Beckman Coulter B.V.) for 3 h at 37 °C in a humidified atmosphere and 5% CO_2. Following this procedure, which initiated apoptosis in approximately 40–50% of the cells, cells were harvested and resuspended in Ca^{2+}-containing binding buffer to a final concentration of 2.5×10^6 cells/mL. Next, the cell suspensions were incubated with the Cy5.5-labeled annexin A5- or control-micelles for 30 min at a final concentration of 1 mM total lipid. An additional apoptotic cell sample was left untreated for comparison. Incubations were performed on a roller bench at room temperature. After the incubation procedure, cells were collected and washed at least three times in 2 mL of Ca^{2+}-containing binding buffer (300 × *g*, 5 min). Last, cells were fixed in 200 μL of 4% paraformaldehyde containing 2.5 mM $CaCl_2$.

For confocal laser scanning microscopy (CLSM), 5 μL of the resuspended fixed cell pellets were applied to poly(L-lysine) microscopy slides (Menzel-Gläser) and dried for 20 min at 55 °C. Next, the adhered cells were washed in PBS, counterstained for nuclei with DAPI (15 min; 0.1 μg/mL in PBS), washed in PBS, and mounted with Mowiol mounting medium. CLSM was performed on a Zeiss LSM 510 META NLO system (Carl Zeiss AG, Oberkochen, Germany), equipped with a multiphoton Chameleon laser and a HeNe633 laser. The Chameleon laser (780 nm) allowed excitation of DAPI, whereas the HeNe633

laser (633 nm) was used for Cy5.5 excitation. All images were obtained at 630× magnification, and imaging settings remained unchanged to allow a direct comparison of the different samples.

In Vivo Experiments

Animals—A total of 10 ApoE$^{-/-}$ and 2 wild-type (WT) male C57BL/6 mice were included for in vivo MRI experiments and additional ex vivo fluorescence imaging or microscopy. One additional apoE$^{-/-}$ mouse was included for ex vivo fluorescence imaging only. ApoE$^{-/-}$ mice were placed on a high-cholesterol diet (0.2% total cholesterol, Harlan Teklad, Madison, Wis) ad libitum beginning at 6 weeks until 60 to 68 weeks of age, while WT mice were maintained on a normal murine diet (Research Diets, Inc., New Brunswick, NJ). All animal experiments were approved by the ethics committee of Mount Sinai General Hospital.

MRI—In vivo MRI measurements were performed with an 89 mm vertical bore MRI system, operating at 9.4T (Bruker Instruments, Billerica, MA, USA). Mice were initially anesthetized with 4% isoflurane in oxygen (0.4 L/min) and placed head-up in a 30 mm birdcage coil for imaging (Bruker). During MRI, anesthesia was maintained using 1.5–2.0% isoflurane in oxygen (0.4 L/min) supplied through a face mask. The respiratory signal was monitored using a pressure sensor to regulate the depth of the anesthesia.

At the onset of the experiment, precontrast T_1-weighted images of the abdominal aorta in the area between the renal and aortic bifurcations were acquired using a fat-suppressed black blood spin–echo sequence with the following parameters: TR = 800 ms, TE = 8.6 ms, NEX = 16, matrix = 256 × 256, FOV = 2.6 × 2.6 cm^2, and slice thickness = 0.5 mm. For flow suppression, an inflow saturation slab of 4 mm, consisting of a 90° pulse followed by a 2 ms spoiler gradient, was positioned superior to the imaging area.

Following the precontrast scans, anesthetized mice were injected with the micellar contrast agent through the tail vein at a dose of 2.5 μmol per mouse (100 μL; 25 mM total lipid concentration). A total of 6 ApoE$^{-/-}$ mice received annexin A5-micelles fluorescently labeled with either Rhodamine-PE (n = 3) or Cy5.5-PEG2000-DSPE (n = 3). control-micelles were administrated to four ApoE$^{-/-}$ mice (Rhodamine-PE, n = 2; Cy5.5-PEG2000-DSPE, n = 2) and two WT mice received Cy5.5-labeled annexin A5-micelles.

At 24 h post-administration of the contrast agent, mice were again prepared for MR measurements. First, imaging slices were carefully matched to the precontrast images by using the unique anatomy of individual vertebrae as anatomical landmarks. Next, T_1-weighted MR images were obtained with the same parameters as used for the precontrast scans. For two ApoE$^{-/-}$ mice, the same MR protocol was additionally repeated at 48 h and 7 days after injection of the annexin A5-micelles.

Mice that underwent their last MR measurement at 24 h post-injection were immediately sacrificed by saline perfusion after the scanning procedure. Blood samples were obtained, and spleen, liver, kidney, and lung tissues were removed to investigate nanoparticle biodistribution. The abdominal aortas from mice that received Rhodamine-labeled micelles were isolated using microscopic dissection and snap-frozen in optical cutting temperature compound (Tissue Tek, Sakura Finetech) for confocal fluorescence microscopy (n = 2/group). Alternatively, whole aortas from mice that received Cy5.5-labeled micelles were excised and placed on a microscopy slide for near-infrared fluorescence imaging (NIRF, n = 2/group). For the latter procedure, the fat surrounding the abdominal aorta was carefully removed.

MR Data Analysis—Images were analyzed using *Mathematica 6* (Wolfram Research, Inc., USA). Prior to analysis, pre- and 24 h postcontrast injection measured slices were matched by the shape of the vertebrae. Slices that could not be matched were excluded from data analysis. Typically, for each ApoE$^{-/-}$ mouse 15 to 19 slices with orientations perpendicular to the abdominal aorta were analyzed. Circular regions of interest (ROIs) were drawn on the pixels in the thickened atherosclerotic vessel wall surrounding the lumen (S_w), while excluding the vessel lumen. A second ROI was drawn in a portion of the surrounding muscle (S_m). Wall signal was divided by the muscle signal to yield a normalized signal intensity $S_{norm} = S_w/S_m$ that could be compared pre- and 24 h post-contrast, as well as between mice. Signal enhancement (SE) was calculated as the average percentile difference between S_{norm} of all pre- and 24 h post-contrast slices: $[(S_{norm\_post} - S_{norm\_pre})/(S_{norm\_pre})] \times 100\%$. WT mice were not analyzed using the above procedure, as the aortic wall in these animals could not be discriminated from surrounding tissue. Alternatively, images from WT mice were visually inspected for possible signal enhancement in the aortic wall.

Near Infrared Fluorescence Imaging—For whole-aorta near-infrared fluorescence imaging (NIRF) 1 ApoE$^{-/-}$ mouse, which received no contrast agent, was used as a control. Aortas from ApoE$^{-/-}$ mice that were injected with either control-micelles ($n = 2$) or annexin A5-micelles ($n = 2$) were collected following the in vivo MRI experiments. The dissected aortas were placed on a microscope slide and covered with gauze submerged in PBS, placed at 4 °C, and imaged within 2 h. Aortas were placed in the IVIS 200 system (Xenogen) and the Cy5.5 label was excited using a wavelength filter with a range of 615–665 nm, while the emission was recorded using a 695–770 nm filter. Fluorescent reflectance images were acquired with identical exposure times for all groups. Total photon count was determined within identical windows around the whole aorta. The mean increase in fluorescence intensity was calculated as the average percentile difference between the total photon count from the contrast-receiving group (PC_{CA}) and the total photon count from the control ApoE$^{-/-}$ mouse that received no contrast agent ($PC_{control}$): $[(PC_{CA} - PC_{control})/(PC_{control})] \times 100\%$.

Confocal Fluorescence Microscopy—8-μm-thick frozen tissue sections were cut for confocal microscopy. Individual sections were air-dried for 10 min and blocked (PBS containing 1% BSA and 5% horse serum) for 45 min at room temperature. DNA fragmentation was detected with the TdT-mediated dUTP Nick End Labeling (TUNEL) technique, using the In Situ Cell Death Detection Kit with fluorescein isothiocyanate (FITC)-labeled dUTP (Roche, Mannheim, Germany) according to manufacturer instructions. Cells with fragmented DNA will be referred to as apoptotic. Macrophages were fluorescently stained with Alexa 647 labeled anti-CD68 antibodies (Serotec, Inc.). After washing with PBS, the sections were directly mounted with VectaShield containing 1.5 μg/mL DAPI (VectorLaboratories, Burlingame, CA) to stain cell nuclei. The sections were covered with coverslips and imaged within 12 h.

Rhodamine-labeled annexin A5-micelles and control-micelles (red) were detected and co-localized with respect to both DNA fragmentation (green) and macrophages (green) within the vessel wall 24 h after contrast agent administration using confocal laser scanning microscopy (Zeiss LSM 510 META microscope, Carl Zeiss AG, Oberkochen, Germany) in an inverted configuration. The system was equipped with four lasers and three confocal detectors, and data were captured and analyzed using Zeiss LSM 510 Meta and postprocessed with *Image Browser* software (Carl Zeiss AG, Oberkochen, Germany). All images were obtained with the same laser power and detector gain settings.

Statistics—Statistical analysis was performed for experiments with $n \geq 3$ per group. Comparisons between the two groups were performed with a Student's t test for independent samples in SPSS 16.0. $P < 0.05$ was considered significant.

RESULTS

Characterization of the Micelles

The hydrodynamic diameters of control and anxA5-micelles were 19.5 ± 0.7 nm and 22.3 ± 0.2 nm, respectively. Protein and phosphate determinations showed that on average two annexin A5-cys proteins were covalently conjugated per micelle, assuming that each micellar nanoparticle contains approximately 80 lipids (37). Based on the initial lipid composition, this also implies that each micelle contains approximately 1 fluorescent dye and 40 gadolinium-based lipids. The potency of a MRI contrast agent to reduce the intrinsic tissue T_1 and T_2 relaxation times, and thereby introduce tissue contrast on MR images, is described by the relaxivity values r_1 and r_2, which are expressed in $mM^{-1}\ s^{-1}$. Relaxivities r_1 and r_2 of the paramagnetic Cy5.5-labeled control-micelles and annexin A5-micelles were measured at 60 MHz and different temperatures. Importantly, similar r_1 and r_2 values were observed for the targeted versus the nontargeted micelles (Table 1). At 25 °C, the relaxivities of control-micelles were $r_1 = 11.8 \pm 0.1\ mM^{-1}\ s^{-1}$ and $r_2 = 18.5 \pm 0.1\ mM^{-1}\ s^{-1}$, whereas for annexin A5-micelles relaxivities were $r_1 = 11.4 \pm 0.1\ mM^{-1}\ s^{-1}$ and $r_2 = 19.4 \pm 0.1\ mM^{-1}\ s^{-1}$. These values, which are based on gadolinium concentration, are relatively high compared to clinically approved gadolinium complexes such as Gd-DTPA, for which $r_1 = 3.3$ and $r_2 = 3.9$ at 1.5 T (64 MHz) and 37 °C (38). An increase in temperature to 37 °C was shown to slightly elevate r_1 and r_2 for both micellar agents (Table 1).

In Vitro Targeting

Ellipsometry measurements clearly demonstrated binding of the annexin A5-micelles to a bilayer consisting of 20 mol % PS and 80 mol % phosphatidylcholine (PC), as observed by the gradually increasing polarization angle, which is known to correlate with layer thickness. The polarization angle reached a steady state at higher values compared to free annexin A5-cys (Figure 2). Binding was shown to strictly depend on annexin A5 as the polarization angle remained at baseline levels after addition of control-micelles. Furthermore, association was Ca^{2+}-dependent, as annexin A5-cys, as well as annexin A5-micelles, instantly dissociated from the bilayer upon addition of Ca^{2+}-chelating EDTA.

Micelle binding to PS-expressing cells was also examined on a Jurkat cell line using confocal laser scanning microscopy (CLSM). Apoptotic cell suspensions that were untreated (Figure 3A) or incubated with control-micelles (Figure 3B) exhibited negligible levels of Cy5.5 fluorescence, while apoptotic cells incubated with the annexin A5-micelles showed a clear cell-associated Cy5.5 signal (Figure 3C).

MRI and NIRF

In vivo precontrast T_1-weighted MR images of atherosclerotic $ApoE^{-/-}$ mice clearly revealed extensive atherosclerotic lesions in their abdominal aorta (Figure 4A,C), whereas aortas of wild-type (WT) C57BL/6 mice showed normal vessel wall morphology within the same region (Figure 4E). At 24 h post-injection of annexin A5-micelles, T_1-weighted images of the same $ApoE^{-/-}$ mice showed increased signal intensity within the thickened aortic vessel wall (compare Figure 4C and D). Contrast enhancement within these mice persisted up to at least 7 days after injection (data not shown). Atherosclerotic lesions of $ApoE^{-/-}$ mice that were injected with control-micelles showed less signal enhancement at 24 h post-

injection (compare Figure 4A and B). Moreover, no contrast changes were observed in WT mice that received annexin A5-micelles (compare Figure 4E and F).

Ex vivo near-infrared fluorescence imaging was performed on excised aortas from ApoE$^{-/-}$ mice that underwent in vivo MRI experiments and were sacrificed 24 h post-contrast agent injection. The aorta of an ApoE$^{-/-}$ mouse that received no contrast agent served as a control and showed marginal fluorescence signal due to autofluorescence (Figure 5A). In contrast, the aortas from ApoE$^{-/-}$ mice that received control-micelles (Figure 5B) or annexin A5-micelles (Figure 5C) displayed strong fluorescence signal, which was heterogeneously distributed over the entire aorta. Interestingly, aortas from mice injected with annexin A5-micelles showed multiple intense fluorescent hotspots, whereas aortas from the control micelle group revealed considerably less fluorescence in a reduced number of areas. Importantly, these hotspots were predominantly observed in areas where extensive atherosclerotic lesions were expected as described by Nakashima et al. (39). These areas included the aortic arch, the branching points of the renal arteries, and the aortic bifurcation (Figure 5C).

MR signal enhancement in the aortic wall also appeared highly heterogeneous throughout the examined abdominal area. Nevertheless, all slices that were measured with in vivo MRI were used to calculate the mean signal enhancement within the vessel wall to prevent any bias by analyzing only specific slices. Mean MR signal within the examined abdominal aortic wall was calculated to be increased by 6.7 ± 3.4% and 10.7 ± 1.7% at 24 h post-administration of control or annexin A5-micelles, respectively (Figure 6A). At the same time point, the total photon count in the entire aorta was enhanced by 113.1 ± 4.4% for the control micelle group and 257.1 ± 9.1% for the annexin A5-micelle group (Figure 6B).

Confocal Fluorescence Microscopy

Tissue sections from the abdominal aortas of the mice were examined with confocal fluorescence microscopy. Atherosclerotic lesions from ApoE$^{-/-}$ mice injected with Rhodamine-labeled control-micelles demonstrated only weak and diffuse red fluorescent signal at 24 h post-injection (Figure 7A,B), whereas bright red fluorescent hot spots were observed for ApoE$^{-/-}$ mice that received annexin A5-micelles (Figure 7C and D). In these latter mice, the annexin A5-micelles clearly colocalized with macrophages (Figure 7C) and apoptotic cells (Figure 7D) in the center of the intima. Presumably, a fraction of these macrophages are apoptotic, as previously described elsewhere (17). No obvious association to macrophages (Figure 7A) or apoptotic cells was observed for control-micelles (Figure 7B).

Biodistribution

At 24 h post-injection of control-micelles in ApoE$^{-/-}$ mice, the Gd content of liver and spleen was shown to be higher than that of kidneys and lungs (Figure 8A). Similar amounts of Gd were measured in the kidneys and lungs of mice that received the annexin A5-functionalized micellar contrast agent (Figure 8B). In contrast, Gd content in the liver and spleen of these mice was approximately 100% and 219% higher, respectively, compared to control-micelles. These results are in agreement with previous studies that demonstrated PS specific uptake of radiolabeled annexin A5 by the liver and spleen, while kidney accumulation appeared to be nonspecific (40). Importantly, preliminary studies in ApoE$^{-/-}$ mice, which were injected with the same contrast agents at equal dose, displayed similar blood clearance kinetics for control and annexin A5-micelles (data not shown). Consequently, this allows a direct comparison of the collected data from both agents.

DISCUSSION

In the current study, we developed, characterized, and evaluated the use of annexin A5-conjugated micelles for targeted MRI of atherosclerotic plaques in ApoE$^{-/-}$ mice. The micelles were composed of a paramagnetic amphiphile (Gd-DTPA-DSA) and PEGylated lipids (PEG-DSPE) in a 1:1 molar ratio. Above the so-called critical micelle concentration (CMC), PEG-DSPE forces the amphiphilic aggregation towards a micellar morphology. A near-infrared fluorophore (Cy5.5) and annexin A5 proteins were covalently conjugated to the distal ends of the PEG chains of the micelles for fluorescence imaging and target specificity, respectively. Alternatively, Rhodamine-PE, instead of Cy5.5-PEG2000-DSPE, was incorporated in the lipid monolayer for confocal fluorescence microscopy. Ellipsometry measurements on PS/PC bilayers and experiments with apoptotic Jurkat cells were performed to assess the target-specificity of the annexin A5-micelles in vitro. Furthermore, in vivo MRI of the abdominal aortas from apoA$^{-/-}$ mice and ex vivo fluorescence methods on excised aortas of the same mice were used to image the uptake of control and annexin A5-micelles in atherosclerotic lesions, as well as to validate their cellular targets following intravenous injection.

MR molecular imaging of vascular targets is usually done with nanoparticles that carry a high payload of contrast-generating material (41, 42). After intravenous administration, such nanoparticulate agents do not require extravasation from the vasculature to bind to their target, and therefore, nanoparticle size is less critical. However, when extravascular targeting is to be accomplished, e.g. in case of intraplaque targeting, a small particle size is more favorable, to allow penetration of the endothelium. Recently, Burtea et al. reported on a novel PS-specific peptide that was conjugated to a single Gd-DTPA, which successfully allowed MRI of PS exposing cells in atherosclerotic plaques (43). Furthermore, Schellenberger et al. reported on a PS-specific superparamagnetic iron oxide-based MRI contrast agent with a hydrodynamic diameter of approximately 15 nm, i.e. annexin A5-VSOP (44). However, this nanoparticle was only applied in an in vitro setting. In the current study, we developed and applied annexin A5-functionalized paramagnetic micellar nanoparticles of similar size. This relatively small size facilitates extravasation in areas with enhanced endothelial permeability, such as atherosclerotic lesions.

Ellipsometry measurements revealed a Ca^{2+}-dependent affinity of the annexin A5-conjugated micelles for a lipid bilayer that contained 20% PS, whereas nonspecific control-micelles did not bind to a similar bilayer. These results were corroborated by CLSM images of apoptotic cells, which showed abundant association of annexin A5-functionalized micelles, whereas control-micelles were barely detected.

For in vivo MRI experiments, we used a dosage that is typical for targeted MR contrast agents, i.e., 50 μmol Gd per kilogram of body weight. MRI revealed pronounced and heterogeneously distributed hyperintense areas throughout plaque-rich regions in the abdominal aorta at 24 h after administration of annexin A5-functionalized micelles. Such enhanced regions were also observed in the untargeted control micelle group, but to a lower extent. To enable comparison of both groups, the signal enhancement for each slice was calculated and averaged for all acquired imaging slices, thereby disregarding heterogeneous distribution of the contrast agent. Data analysis revealed that the mean signal enhancement throughout the abdominal aorta was nonsignificantly higher for mice that received annexin A5-micelles than for control micelle-injected mice. In both cases, the enhancement was, however, modest compared to macrophage scavenger receptor (MSR) targeted micellar contrast agents that were applied at a dose of 75 μmol Gd per kilogram of body weight (26).

In vivo MRI observations were compared to ex vivo fluorescence imaging of excised aortas. The mean photon count of aortas that originated from mice injected with annexin A5-micelles was at least twice that of the aortas from control micelle injected mice. In addition, near-infrared fluorescence imaging allowed us to investigate the entire aorta. The most pronounced uptake of annexin A5-micelles was observed in the aortic arch, at principal branches of the abdominal aorta, such as the renal arteries, and at the aortic bifurcation into the iliac arteries. Isobe et al. observed distinct uptake of ^{99m}Tc-labeled annexin A5 in similar regions of the aorta in ApoE$^{-/-}$ mice (17). Importantly, these regions are known to correspond to a high plaque burden (39), which was the case in this study as well. However, one should note that the in vivo MR images were acquired in the abdominal aorta in the area between the renal and aortic bifurcations. This implies that certain regions with intense uptake of the micellar contrast agent were not included in the in vivo MRI scans, which could partially explain the observed difference in signal enhancement between MRI and NIRF imaging. Future imaging studies should therefore cover a larger area of the abdominal aorta, or alternatively, another animal model could be used, with well-defined locations and phenotype of atherosclerotic plaque within the carotid artery (45).

Ex vivo confocal fluorescence microscopy revealed association of annexin A5-micelles to PS-expressing cells, such as apoptotic cells and macrophages, within atherosclerotic lesions in the abdominal aorta. A large fraction of these apoptotic cells are considered dying macrophages, whereas the remaining fraction most likely consists of smooth muscle cells (46). The annexin A5-functionalized contrast agent was most probably also associated with viable macrophages, as previously observed for biotinylated annexin A5 (17). Macrophages in atherosclerotic lesions are also known to nonspecifically engulf nanoparticulate agents such as USPIOs (47). Nevertheless, CLSM images of tissue sections from control micelle-injected mice revealed no macrophage-associated micellar fluorescence. Presumably, the cell-associated contrast agents observed in the CLSM images were internalized, which may have led to a quenched T_1 effect due to limited water exchange with the bulk (48, 49). Such an effect may provide a second explanation for the apparent discrepancy between the modest signal enhancement of annexin A5-micelles in the in vivo MR images and the large difference in micellar fluorescence from control and annexin A5-micelles in the ex vivo CLSM images.

At present, there is an urgent need to discriminate vulnerable atherosclerotic lesions from stable lesions. Current diagnostic methods used in the clinic are primarily focused on visualizing narrowing of the lumen but do not reveal plaque composition and thus do not predict the risk of rupture accurately (23). In the past decade, traditional high-resolution MRI techniques have been developed to enable plaque characterization by visualizing features such as the lipid-rich core and fibrous cap size. The biochemistry that lies at the basis of plaque formation may be investigated using MRI-based molecular imaging techniques. For example, MR imaging of the macrophage burden has been investigated with ultrasmall iron oxide nanoparticles (USPIO) (47), while the expression of cell adhesion molecules was visualized using VCAM-1 targeted cross-linked iron oxide nanoparticles (CLIO) (31). Furthermore, annexin A5-functionalized iron oxide particles were applied to image PS-expressing cells in a preliminary study on a limited number of animals (50). The disadvantage of such strategies is that iron oxide-based imaging relies on the use of so-called $T_2^{(*)}$-weighted MRI, in which regions of high iron oxide content appear dark. These spots are hard to localize in images that usually already have a low signal-to-noise ratio. Therefore, more recent investigations primarily focus on the application of T_1-reducing agents that appear bright in T_1-weighted MR images (25, 29, 43), as is the case in our study. The paramagnetic nanoparticulate agent introduced in the present study exhibited enhanced accumulation in plaque by the conjugation of annexin A5. This phenomenon may also be

applied to shuttle therapeutically active compounds, such as anti-inflammatory agents or nucleotides, into plaque.

In the present study, a dose of 1.9 mg annexin A5 was administered per mouse, which was well tolerated by the animals. However, this dose is considered unfeasible in clinical studies. Ideally, small molecules such as peptides or peptidomimetics, with a high affinity for PS, need to be developed for clinical translation. Alternatively, and despite the previously mentioned disadvantages, small iron oxide nanoparticles may be employed. These nanoparticles represent a more sensitive MRI contrast agent and are typically injected at a 100-fold lower particle dose, which also decreases the Annexin A5 dose by a factor 100.

In conclusion, the present study demonstrated the potential of an annexin A5-functionalized micellar contrast agent for target-specific imaging of PS-expressing cells in atherosclerotic lesions of ApoE$^{-/-}$ mice. Such imaging strategies are of great diagnostic potential as the abundance of PS expressing cells is considered an important prognostic marker of plaque vulnerability. Interestingly, the presented nanoparticulate platform may be simultaneously exploited for therapeutic purposes, thereby facilitating a wide range of clinically relevant applications for improved diagnostics, as well as therapeutic interventions in atherosclerotic cardiovascular disease.

Acknowledgments

This project was funded by the BSIK program entitled Molecular Imaging of Ischemic Heart Disease (project number BSIK03033). Part of this research was funded by the ED-FP6-project DiMI, LSHB-CT-2005-512146, and carried out within the framework of the European Cooperation in the field of Scientific and Technical Research (COST) D38 Action Metal Based Systems for Molecular Imaging Applications. Furthermore, this research was supported by a travel grant awarded by The Netherlands Organization for Scientific Research (NWO). Part of this work was supported by European Union grant Euregional PACT II (IVA-VLANED-1.20).

LITERATURE CITED

1. Andree HA, Reutelingsperger CP, Hauptmann R, Hemker HC, Hermens WT, Willems GM. Binding of vascular anticoagulant alpha (VAC alpha) to planar phospholipid bilayers. J. Biol. Chem. 1990; 265:4923–4928. [PubMed: 2138622]
2. Gerke V, Moss SE. Annexins: from structure to function. Physiol. Rev. 2002; 82:331–371. [PubMed: 11917092]
3. Devaux PF, Zachowski A. Maintenance and consequences of membrane phospholipid asymmetry. Chem. Phys. Lipids. 1994; 73:107–120.
4. Zwaal RF, Comfurius P, Bevers EM. Surface exposure of phosphatidylserine in pathological cells. Cell. Mol. Life Sci. 2005; 62:971–988. [PubMed: 15761668]
5. Schroit AJ, Zwaal RF. Transbilayer movement of phospholipids in red cell and platelet membranes. Biochim. Biophys. Acta. 1991; 1071:313–329. [PubMed: 1958692]
6. Callahan MK, Williamson P, Schlegel RA. Surface expression of phosphatidylserine on macrophages is required for phagocytosis of apoptotic thymocytes. Cell Death Differ. 2000; 7:645–653. [PubMed: 10889509]
7. van Engeland M, Nieland LJ, Ramaekers FC, Schutte B, Reutelingsperger CP. Annexin V-affinity assay: a review on an apoptosis detection system based on phosphatidylserine exposure. Cytometry. 1998; 31:1–9. [PubMed: 9450519]
8. Halbreich A, Roger J, Pons JN, Geldwerth D, Da Silva MF, Roudier M, Bacri JC. Biomedical applications of maghemite ferrofluid. Biochimie. 1998; 80:379–390. [PubMed: 9782379]
9. Vermes I, Haanen C, Reutelingsperger C. Flow cytometry of apoptotic cell death. J. Immunol. Methods. 2000; 243:167–190. [PubMed: 10986414]
10. Boersma HH, Kietselaer BL, Stolk LM, Bennaghmouch A, Hofstra L, Narula J, Heidendal GA, Reutelingsperger CP. Past, present, and future of annexin A5: from protein discovery to clinical applications. J. Nucl. Med. 2005; 46:2035–2050. [PubMed: 16330568]

11. Kenis H, Hofstra L, Reutelingsperger CP. Annexin A5: shifting from a diagnostic towards a therapeutic realm. Cell. Mol. Life Sci. 2007; 64:2859–2862. [PubMed: 17876516]
12. Davies MJ, Richardson PD, Woolf N, Katz DR, Mann J. Risk of thrombosis in human atherosclerotic plaques: role of extracellular lipid, macrophage, and smooth muscle cell content. Br. Heart J. 1993; 69:377–381. [PubMed: 8518056]
13. Kolodgie FD, Narula J, Burke AP, Haider N, Farb A, Hui-Liang Y, Smialek J, Virmani R. Localization of apoptotic macrophages at the site of plaque rupture in sudden coronary death. Am. J. Pathol. 2000; 157:1259–1268. [PubMed: 11021830]
14. Libby P, Geng YJ, Aikawa M, Schoenbeck U, Mach F, Clinton SK, Sukhova GK, Lee RT. Macrophages and atherosclerotic plaque stability. Curr. Opin. Lipidol. 1996; 7:330–335. [PubMed: 8937525]
15. Li W, Hellsten A, Jacobsson LS, Blomqvist HM, Olsson AG, Yuan XM. Alpha-tocopherol and astaxanthin decrease macrophage infiltration, apoptosis and vulnerability in atheroma of hyperlipidaemic rabbits. J. Mol. Cell Cardiol. 2004; 37:969–978. [PubMed: 15522274]
16. Kolodgie FD, Petrov A, Virmani R, Narula N, Verjans JW, Weber DK, Hartung D, Steinmetz N, Vanderheyden JL, Vannan MA, Gold HK, Reutelingsperger CP, Hofstra L, Narula J. Targeting of apoptotic macrophages and experimental atheroma with radiolabeled annexin V: a technique with potential for noninvasive imaging of vulnerable plaque. Circulation. 2003; 108:3134–3139. [PubMed: 14676140]
17. Isobe S, Tsimikas S, Zhou J, Fujimoto S, Sarai M, Branks MJ, Fujimoto A, Hofstra L, Reutelingsperger CP, Murohara T, Virmani R, Kolodgie FD, Narula N, Petrov A, Narula J. Noninvasive imaging of atherosclerotic lesions in apolipoprotein E-deficient and low-density-lipoprotein receptor-deficient mice with annexin A5. J. Nucl. Med. 2006; 47:1497–1505. [PubMed: 16954559]
18. Haider N, Hartung D, Fujimoto S, Petrov A, Kolodgie FD, Virmani R, Ohshima S, Liu H, Zhou J, Fujimoto A, Tahara A, Hofstra L, Narula N, Reutelingsperger C, Narula J. Dual molecular imaging for targeting metal-loproteinase activity and apoptosis in atherosclerosis: molecular imaging facilitates understanding of pathogenesis. J. Nucl. Cardiol. 2009; 16:753–762. [PubMed: 19662466]
19. Hartung D, Sarai M, Petrov A, Kolodgie F, Narula N, Verjans J, Virmani R, Reutelingsperger C, Hofstra L, Narula J. Resolution of apoptosis in atherosclerotic plaque by dietary modification and statin therapy. J. Nucl. Med. 2005; 46:2051–2056. [PubMed: 16330569]
20. Sarai M, Hartung D, Petrov A, Zhou J, Narula N, Hofstra L, Kolodgie F, Isobe S, Fujimoto S, Vanderheyden JL, Virmani R, Reutelingsperger C, Wong ND, Gupta S, Narula J. Broad and specific caspase inhibitorinduced acute repression of apoptosis in atherosclerotic lesions evaluated by radiolabeled annexin A5 imaging. J. Am. Coll. Cardiol. 2007; 50:2305–2312. [PubMed: 18068039]
21. Kietselaer BL, Reutelingsperger CP, Heidendal GA, Daemen MJ, Mess WH, Hofstra L, Narula J. Noninvasive detection of plaque instability with use of radiolabeled annexin A5 in patients with carotid-artery atherosclerosis. N. Engl. J. Med. 2004; 350:1472–1473. [PubMed: 15070807]
22. Cappendijk VC, Cleutjens KB, Kessels AG, Heeneman S, Schurink GW, Welten RJ, Mess WH, Daemen MJ, van Engelshoven JM, Kooi ME. Assessment of human atherosclerotic carotid plaque components with multisequence MR imaging: initial experience. Radiology. 2005; 234:487–492. [PubMed: 15671004]
23. Sanz J, Fayad ZA. Imaging of atherosclerotic cardiovascular disease. Nature. 2008; 451:953–957. [PubMed: 18288186]
24. Mulder WJ, Strijkers GJ, van Tilborg GA, Griffioen AW, Nicolay K. Lipid-based nanoparticles for contrast-enhanced MRI and molecular imaging. NMR Biomed. 2006; 19:142–164. [PubMed: 16450332]
25. Amirbekian V, Lipinski MJ, Briley-Saebo KC, Amirbekian S, Aguinaldo JG, Weinreb DB, Vucic E, Frias JC, Hyafil F, Mani V, Fisher EA, Fayad ZA. Detecting and assessing macrophages in vivo to evaluate atherosclerosis noninvasively using molecular MRI. Proc. Natl. Acad. Sci. U.S.A. 2007; 104:961–966. [PubMed: 17215360]

26. Mulder WJ, Strijkers GJ, Briley-Saboe KC, Frias JC, Aguinaldo JG, Vucic E, Amirbekian V, Tang C, Chin PT, Nicolay K, Fayad ZA. Molecular imaging of macrophages in atherosclerotic plaques using bimodal PEGmicelles. Magn. Reson. Med. 2007; 58:1164–1170. [PubMed: 18046703]
27. Cormode DP, Chandrasekar R, Delshad A, Briley-Saebo KC, Calcagno C, Barazza A, Mulder WJ, Fisher EA, Fayad ZA. Comparison of synthetic high density lipoprotein (HDL) contrast agents for MR imaging of atherosclerosis. Bioconjugate Chem. 2009; 20:937–943.
28. Mulder WJ, Douma K, Koning GA, van Zandvoort MA, Lutgens E, Daemen MJ, Nicolay K, Strijkers GJ. Liposome-enhanced MRI of neointimal lesions in the ApoE-KO mouse. Magn. Reson. Med. 2006; 55:1170–1174. [PubMed: 16598732]
29. Winter PM, Morawski AM, Caruthers SD, Fuhrhop RW, Zhang H, Williams TA, Allen JS, Lacy EK, Robertson JD, Lanza GM, Wickline SA. Molecular imaging of angiogenesis in early-stage atherosclerosis with alpha(v)beta3-integrin-targeted nanoparticles. Circulation. 2003; 108:2270–2274. [PubMed: 14557370]
30. Cormode DP, Skajaa T, van Schooneveld MM, Koole R, Jarzyna P, Lobatto ME, Calcagno C, Barazza A, Gordon RE, Zanzonico P, Fisher EA, Fayad ZA, Mulder WJ. Nanocrystal core high-density lipoproteins: a multimodality contrast agent platform. Nano Lett. 2008; 8:3715–3723. [PubMed: 18939808]
31. Nahrendorf M, Jaffer FA, Kelly KA, Sosnovik DE, Aikawa E, Libby P, Weissleder R. Noninvasive vascular cell adhesion molecule-1 imaging identifies inflammatory activation of cells in atherosclerosis. Circulation. 2006; 114:1504–1511. [PubMed: 17000904]
32. Mulder WJ, Griffioen AW, Strijkers GJ, Cormode DP, Nicolay K, Fayad ZA. Magnetic and fluorescent nanoparticles for multimodality imaging. Nanomedicine. 2007; 2:307–324. [PubMed: 17716176]
33. Vermes I, Haanen C, Steffens-Nakken H, Reutelingsperger C. A novel assay for apoptosis. Flow cytometric detection of phosphatidylserine expression on early apoptotic cells using fluorescein labelled Annexin V. J. Immunol. Methods. 1995; 184:39–51. [PubMed: 7622868]
34. van Tilborg GA, Mulder WJ, Deckers N, Storm G, Reutelingsperger CP, Strijkers GJ, Nicolay K. Annexin A5-functionalized bimodal lipid-based contrast agents for the detection of apoptosis. Bioconjugate Chem. 2006; 17:741–749.
35. Rouser G, Fkeischer S, Yamamoto A. Two dimensional thin layer chromatographic separation of polar lipids and determination of phospholipids by phosphorus analysis of spots. Lipids. 1970; 5:494–496. [PubMed: 5483450]
36. Bradford MM. A rapid and sensitive method for the quantitation of microgram quantities of protein utilizing the principle of protein-dye binding. Anal. Biochem. 1976; 72:248–254. [PubMed: 942051]
37. Ashok B, Arleth L, Hjelm RP, Rubinstein I, Onyuksel H. In vitro characterization of PEGylated phospholipid micelles for improved drug solubilization: effects of PEG chain length and PC incorporation. J. Pharm. Sci. 2004; 93:2476–2487. [PubMed: 15349957]
38. Port M, Idee JM, Medina C, Robic C, Sabatou M, Corot C. Efficiency, thermodynamic and kinetic stability of marketed gadolinium chelates and their possible clinical consequences: a critical review. Biometals. 2008; 21:469–490. [PubMed: 18344005]
39. Nakashima Y, Plump AS, Raines EW, Breslow JL, Ross R. ApoE-deficient mice develop lesions of all phases of atherosclerosis throughout the arterial tree. Arterioscler. Thromb. 1994; 14:133–140. [PubMed: 8274468]
40. Tait JF, Smith C, Blankenberg FG. Structural requirements for in vivo detection of cell death with 99mTc-annexin V. J. Nucl. Med. 2005; 46:807–815. [PubMed: 15872355]
41. Mulder WJ, Strijkers GJ, Habets JW, Bleeker EJ, van der Schaft DW, Storm G, Koning GA, Griffioen AW, Nicolay K. MR molecular imaging and fluorescence microscopy for identification of activated tumor endothelium using a bimodal lipidic nanoparticle. FASEB J. 2005; 19:2008–2010. [PubMed: 16204353]
42. Winter PM, Caruthers SD, Kassner A, Harris TD, Chinen LK, Allen JS, Lacy EK, Zhang H, Robertson JD, Wickline SA, Lanza GM. Molecular imaging of angiogenesis in nascent Vx-2 rabbit tumors using a novel alpha(nu)beta3-targeted nanoparticle and 1.5 T magnetic resonance imaging. Cancer Res. 2003; 63:5838–5843. [PubMed: 14522907]

43. Burtea C, Laurent S, Lancelot E, Ballet S, Murariu O, Rousseaux O, Port M, Vander Elst L, Corot C, Muller RN. Peptidic targeting of phosphatidylserine for the MRI detection of apoptosis in atherosclerotic plaques. Mol. Pharm. 2009; 6:1903–1919. [PubMed: 19743879]
44. Schellenberger E, Schnorr J, Reutelingsperger C, Ungethum L, Meyer W, Taupitz M, Hamm B. Linking proteins with anionic nanoparticles via protamine: ultrasmall protein-coupled probes for magnetic resonance imaging of apoptosis. Small. 2008; 4:225–230. [PubMed: 18203233]
45. Cheng C, Tempel D, van Haperen R, van der Baan A, Grosveld F, Daemen MJ, Krams R, de Crom R. Atherosclerotic lesion size and vulnerability are determined by patterns of fluid shear stress. Circulation. 2006; 113:2744–2753. [PubMed: 16754802]
46. Harada K, Chen Z, Ishibashi S, Osuga J, Yagyu H, Ohashi K, Yahagi N, Shionoiri F, Sun L, Yazaki Y, Yamada N. Apoptotic cell death in atherosclerotic plaques of hyperlipidemic knockout mice. Atherosclerosis. 1997; 135:235–239. [PubMed: 9430373]
47. Ruehm SG, Corot C, Vogt P, Kolb S, Debatin JF. Magnetic resonance imaging of atherosclerotic plaque with ultrasmall superparamagnetic particles of iron oxide in hyperlipidemic rabbits. Circulation. 2001; 103:415–422. [PubMed: 11157694]
48. Strijkers GJ, Hak S, Kok MB, Springer CS Jr, Nicolay K. Three-compartment T1 relaxation model for intracellular paramagnetic contrast agents. Magn. Reson. Med. 2009; 61:1049–1058. [PubMed: 19215042]
49. Terreno E, Geninatti Crich S, Belfiore S, Biancone L, Cabella C, Esposito G, Manazza AD, Aime S. Effect of the intracellular localization of a Gd-based imaging probe on the relaxation enhancement of water protons. Magn. Reson. Med. 2006; 55:491–497. [PubMed: 16450336]
50. Smith BR, Heverhagen J, Knopp M, Schmalbrock P, Shapiro J, Shiomi M, Moldovan NI, Ferrari M, Lee SC. Localization to atherosclerotic plaque and biodistribution of biochemically derivatized superparamagnetic iron oxide nanoparticles (SPIONs) contrast particles for magnetic resonance imaging (MRI). Biomed. Microdevices. 2007; 9:719–727. [PubMed: 17562181]

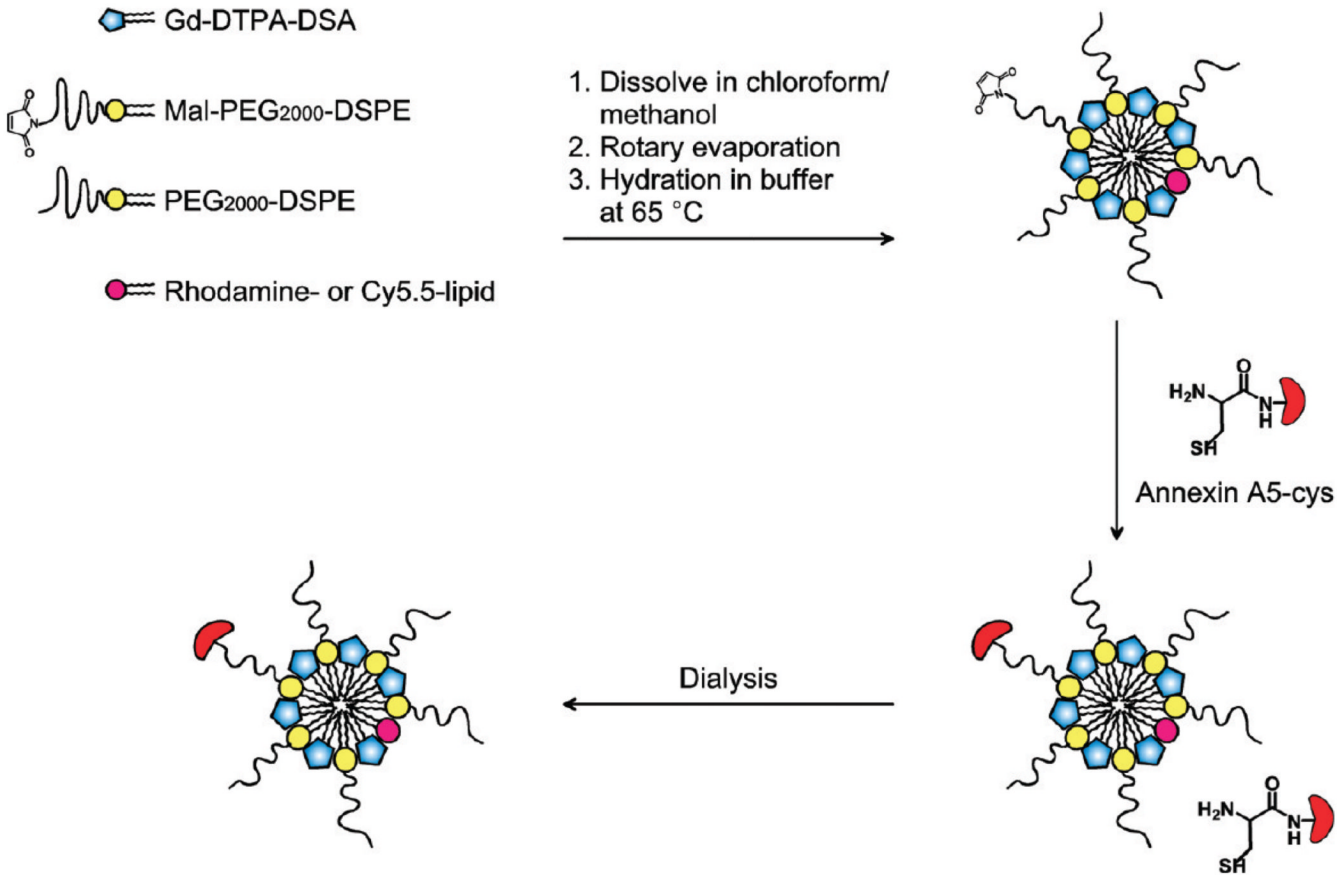

Figure 1.
Schematic of nanoparticle preparation.

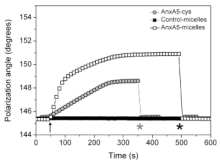

Figure 2.

Ellipsometry measurements of a PS/PC (20:80) bilayer in the presence of 2.5 mM Ca^{2+} upon addition of annexin A5-cys (AnxA5-cys), annexin A5-micelles (AnxA5-micelles), and control-micelles. Micelles or protein was added at the time point indicated by the arrow. 5 mM EDTA was added at the time points indicated by the asterisks (*) to assess Ca^{2+}-dependence of binding.

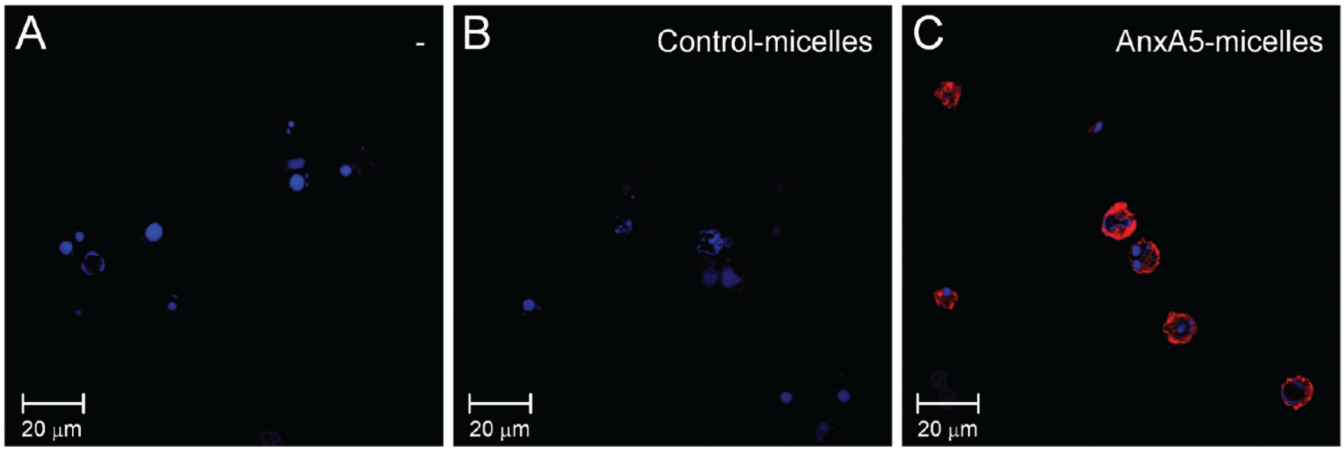

Figure 3.
CLSM images of fixed apoptotic Jurkat cells after incubation with (A) no contrast agent, (B) untargeted paramagnetic control-micelles, or (C) paramagnetic annexin A5-micelles (AnxA5-micelles). Micelles contained Cy5.5-PEG2000-DSPE (red), and adhered cells were counterstained with DAPI (blue). Magnification: 630×.

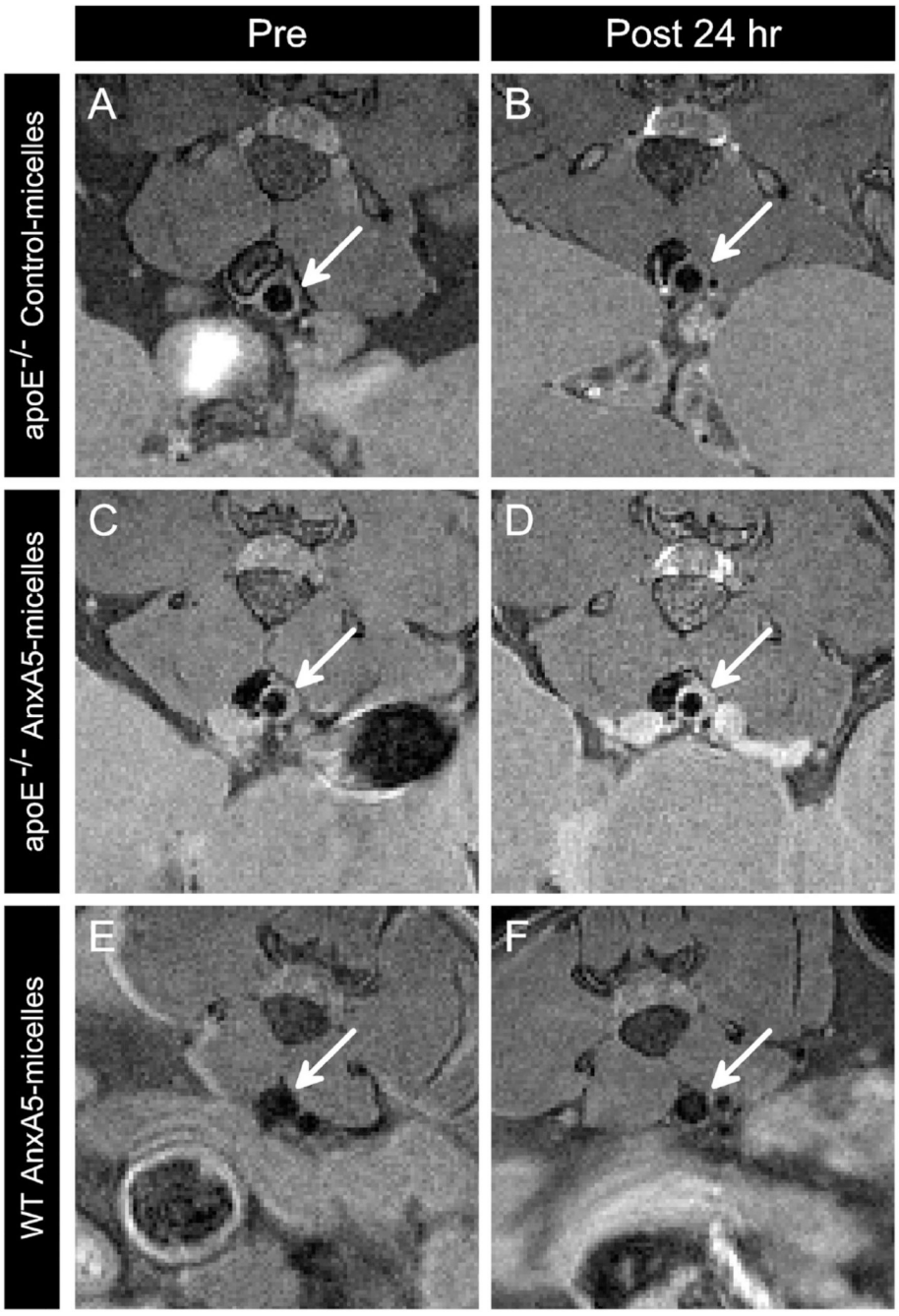

Figure 4.

T_1-weighted in vivo MR images at the level of the abdominal aorta (arrow). Scans were made before (left panel) and 24 h after (right panel) contrast agent injection. ApoE$^{-/-}$ mice received either control-micelles (A,B) or annexin A5-micelles (C,D). Wild-type (WT) C57BL/6 mice only received annexin A5-micelles (E,F).

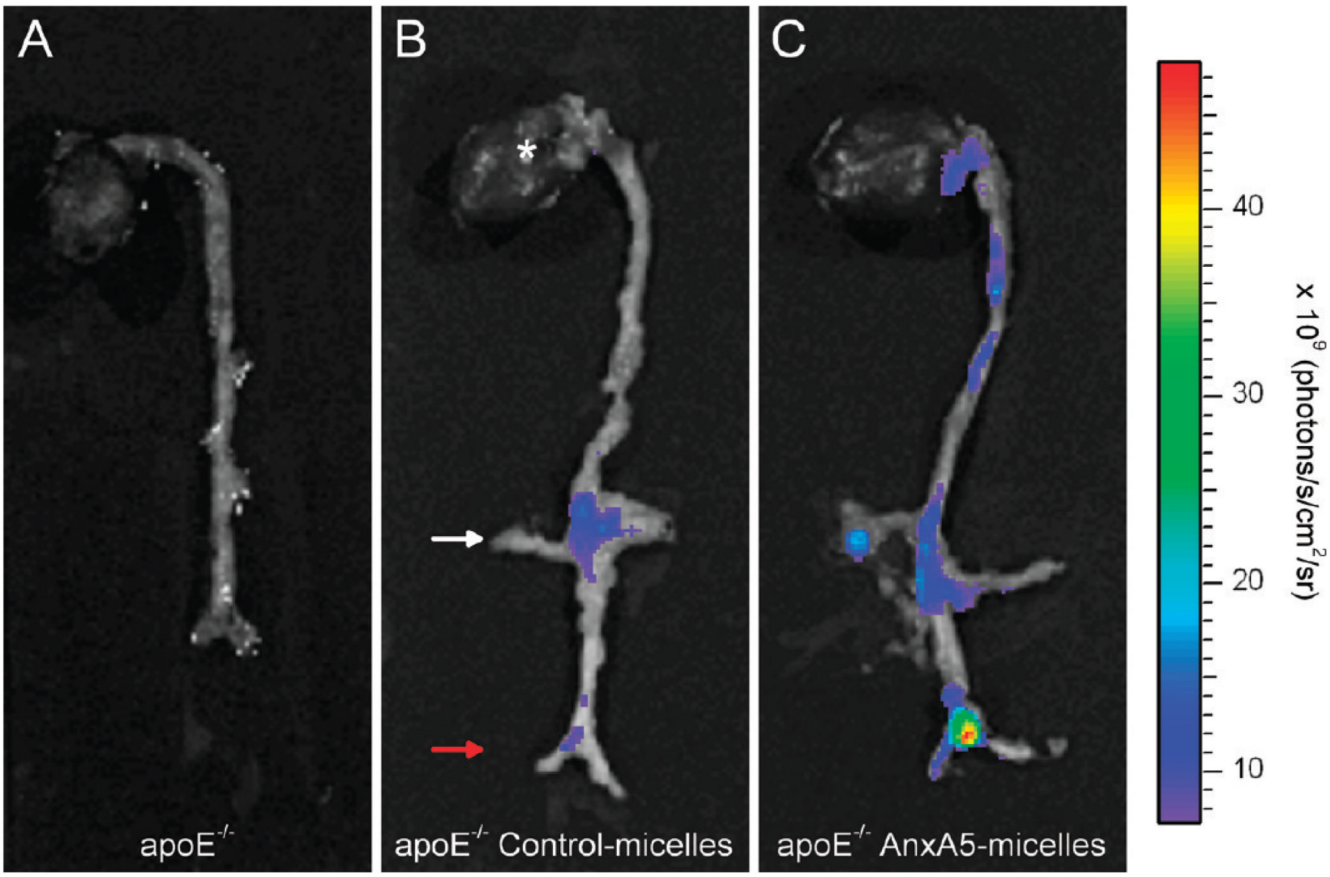

Figure 5.

Ex vivo near-infrared fluorescence imaging (NIRF) of whole aortas from ApoE$^{-/-}$ mice (A) without contrast agent injection and at 24 h after injection of (B) control-micelles and (C) annexin A5-micelles. Micelles contained Cy5.5-PEG2000-DSPE. The orientation of the aorta is indicated by characteristic regions in (B), such as the heart (*), a renal branch (white arrow),and the aortic bifurcation (red arrow). In vivo MR images were acquired in the area between the white and the red arrow.

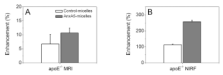

Figure 6.
Quantitative analysis of MR signal enhancement in T_1-weighted images (A) and NIRF enhancement (B) at 24 h after injection of the contrast agent in $ApoE^{-/-}$ mice (B). Bars represent mean values ± SE: (A) MRI: control-micelles (n = 4), annexin A5-micelles (n = 6). NIRF: control-micelles (n = 2), annexin A5-micelles (n = 2).

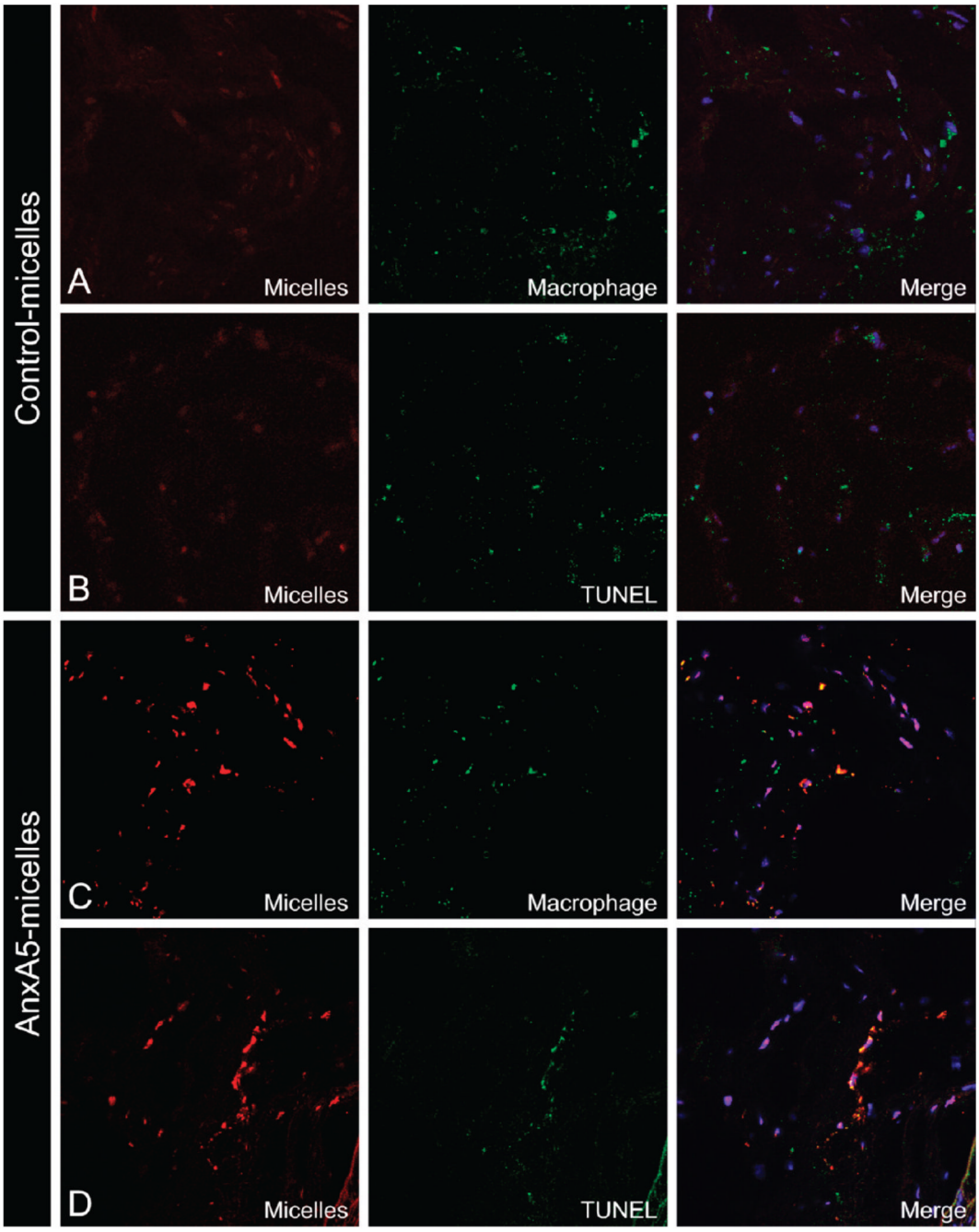

Figure 7.

Confocal fluorescence microscopy of frozen sections from abdominal aortas of ApoE$^{-/-}$ mice at 24 h after administration of (A,B) control-micelles or (C,D) annexin A5-micelles (red). Sections were counterstained for (A,C) macrophages with anti-CD68 (green) or (C,D) apoptotic cells with TUNEL (green). Nuclei were stained with DAPI. Magnification: 400×.

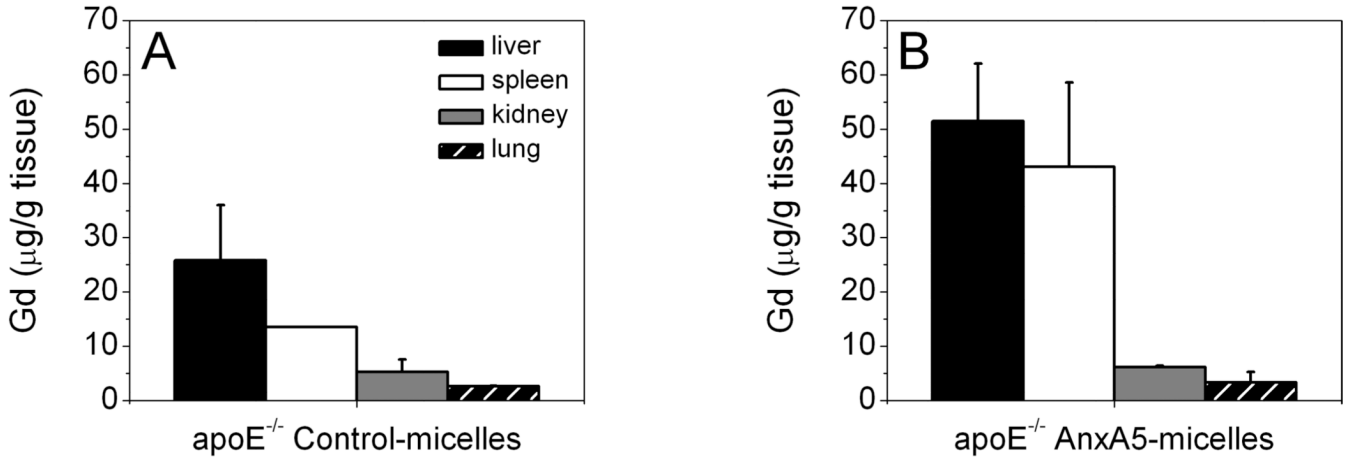

Figure 8.
Biodistribution of control-micelles (A) and annexin A5-micelles (B) at 24 h post-injection in ApoE$^{-/-}$ mice, as measured by ICP-MS of Gd content indicated in micrograms per gram of tissue. Bars represent average ± SD (n = 2/group).

Table 1

Relaxivities of Nonspecific Control-micelles and Annexin A5-Micelles (AnxA5-micelles) in HEPES Buffered Saline at 60 MHz and Different Temperatures[a]

	25 °C		37 °C	
	r_1 (mM^{-1} s^{-1})	r_2 (mM^{-1} s^{-1})	r_1 (mM^{-1} s^{-1})	r_2 (mM^{-1} s^{-1})
Control-micelles	11.8 ± 0.1	18.5 ± 0.1	13.4 ± 0.1	20.4 ± 0.1
AnxA5-micelles	11.4 ± 0.1	19.4 ± 0.1	12.4 ± 0.1	19.9 ± 0.1

[a]Relaxivity values are based on Gadolinium concentration.